Comprehensive Evaluation of Properties of Laser Welded Overlay of Powder H13 Steel on Structural S355 Steel and on H11 Tool Steel

Ivo Černý *, Tomáš Mužík, František Wágner, Jan Kec

Posted Date: 30 March 2026

doi: 10.20944/preprints202603.2365.v1

Keywords: laser welded overlay; powder H13 steel; S355 structural steel; H11 tool steel; fatigue resistance; fatigue damage mechanisms; surface and subsurface defects; residual stresses

 doi:10.20944/preprints202603.2365.v1

Article

Comprehensive Evaluation of Properties of Laser Welded Overlay of Powder H13 Steel on Structural S355 Steel and on H11 Tool Steel

Ivo Černý [1,*], Tomáš Mužík [2], František Wágner [2] and Jan Kec [1]

[1] Strength laboratory SVÚM a.s. Tovární 2053 250 88 Čelákovice, Czech Republic
[2] MATEX PM, Libušínská 60, 326 00 Pilsen, Czech Republic
* Correspondence: ivo.cerny@seznam.cz; Tel.: +420 723 713 718

Abstract

Laser hard overlaying is an advanced, perspective technology with wide industrial applications, for example dies. The aim is to improve surface properties like wear resistance using special layers of powder sintered or remelted by laser beam. At present, dies are manufactured by machining with following bulk heat treatment, which is an expensive process particularly due to use of expensive high-alloyed tool steels. Repairs performed using arc or plasma welding introduce a big amount of heat to the part, which can cause dimension changes and material degradation, These methods often fail also due to low weldability of the materials. An advantage of laser overlaying is minimization of these difficulties. The paper contains a comprehensive evaluation of several types of hard overlayed powder of H13 tool steel on a S355 structural steel and on H11 tool steel using laser beam. Macro- and microstructure, hardness and fatigue resistance are evaluated including fatige damage mechanisms. Results are completed with basic measurement of residual stresses using destructive strain-gauge methods. Fatigue resistance is sensitive on surface and subsurface defects, which can significantly reduce endurance limit.

Keywords: laser welded overlay; powder H13 steel; S355 structural steel; H11 tool steel; fatigue resistance; fatigue damage mechanisms; surface and subsurface defects; residual stresses

1. Introduction

Additive Manufacturing (AM) is a new innovative technology that allows the direct fabrication of complex, individual and high-strength metal products, based on their 3D data. The technology generally refers to processes where the computational design is used for the production of components through the addition of material. Contrary to conventional manufacturing methods, AM is based on production through layer increments [1]. In the AM of metals, metallic powders are totally or partially fused by energy of a laser and transformed by layers into a solid component that has practically no geometric constraints [2].

In spite of numerous advantages of AM like a significant reduction of waste, reduction of manufacture time, reduction of labour costs, an application of AM is connected with numerous challenges. One of the main targets of AM is to manufacture parts to the net-shape or near-net shape, which are characteristic by no or minimal surface processing for targeted applications. This requires an in-depthunderstanding of the formation of various types of AM surfaces, including the variation in surface condition and controlling factors, and their influence on mechanical performance [3].

Fatigue resistance of numerous AM parts has to be considered, as the parts are usually dynamically loaded in service. In this area, a lot of knowledge can be found in the literature. Factors

 doi:10.20944/preprints202603.2365.v1

controlling the fatigue resistance are namely complex, affecting each other. Some examples can be given as follows.

An important factor is surface roughness, particularly, when no additional, final machining is applied. Surface roughness is often affected by the presence of partially molten particles. Surface finishing treatments improve the surface quality and the fatigue life. However, the achievement of the lowest surface roughness does not necessarily correspond to the best fatigue performance, thus suggesting that multiple mechanisms may be active and that besides surface roughness also residual stresses contribute to increase the fatigue strength [4].

Another factor is porosity, which in case of laser powder-bed fusion may depend on different laser velocities [5]. Inappropriate process parameters can cause either under-melting or over-melting. In the former case, lack of fusion and balling defects [6,7] can be formed, whereas in the latter case, keyhole pores [8] and spatter particles [9] are often observed. Under cyclic loading, these pores create local stress concentration and trigger fatigue crack initiation. Results from existing studies highlighted the influence of defects, such as porosity and surface roughness, as the cause for the premature fatigue failure of L-PBF parts [10–13]. AM metal parts are usually characteristic by high strength, which can experience up to a 40% reduction in fatigue performance due to manufacturing defects [14]. It is well known that high strength positively affects fatigue resistance of metals with a low surface roughness and not containing defects. On the other hand, high strength metals are sensitive to crack-like defects and surface microscopic notches, which initiate fatigue cracking, particularly in high-cycle or very high-cycle regimes at low stress amplitudes, when the failure may occur after many cycles. A good indicator of notch sensitivity is fracture toughness [14].

The fact that high strength metals are sensitive to crack-like defects and surface microscopic notches is supported by results published in [15]. The Inconel 718 steel produced by AM had a higher microhardness and higher tensile strength than the forged and rolled material, but its fatigue performance was lower. The steel manufactured by Laser Beam – Powder Bed Fusion (LB-PBF) demonstrated shorter fatigue life, especially under low and medium stresses, i.e. in high-cycle regime. The shorter fatigue life of the material obtained by PBF-LB was attributed to typical process defects besides microstructural differences, in connection to the higher sensitivity to defects.

Effects of Post-Processing Treatments on Fatigue Performance of an alloy manufactured by LB-PBF were studied in [16]. The material was the Ti6Al4V alloy, which is known to be highly susceptible to the notch effect. The material waspost-processed by machining and combinations of alternative mechanical and electrochemical surface treatments. Compressive residual stresses were introduced in all surface-treated samples. After tribofinishing, surface roughness was reduced to 0.31 ± 0.10 μm, which was found to be the most critical factor. It was concluded that machined surfaces presented a fatigue behavior comparable to wrought material. Additionally, alternative surface treatments showed a fatigue behavior equivalent to the casting material.The results concerned the titanium alloy, but can be generalized to other metallic materials.

Another important issue concerning fatigue resistance of additively manufactured metals is the building direction. As an example, the anisotropic fatigue behavior was shown in [17], where an Additively Manufactured AISI 316L Stainless Steel had a higher fatigue strength for horizontally built specimens compared to the vertical building direction. This result can be generalised. Similar results were namely obtained for the 3D printed Inconel 718 Alloy – higher fatigue strength for horizontally built specimens [18].

It can be pointed out as a conclusion that fatigue resistance of Additively Manufactured metals is a complex phenomenon affected by many different factors, often acting mutually. In spite of that computational modelling is being used (e.g. [19]), this field usually needs a lot of experimental works targeted at specific cases of AM with the aim to optimize manufacturing parameters and considering specific service conditions of AM parts and components. The aim of this work is an evaluation of properties of laser welded overlay of powder H13 steel on structural S355 steel, which is a cost effective solution, as the S355 steel is quite a non-expensive material. The second part of the project concerned welded overlay of powder H13 and on H11 tool steel, which is important particularly for

 doi:10.20944/preprints202603.2365.v1

repairs of tools and dies. The technologies are to be used for an advanced, low costs and effective manufacture of tools with a high temperature and high wear resistance like dies and for repairing such tools. As these tools are usually loaded also dynamically besides wear, the investigation described in this article was targeted on fatigue properties.

2. Materials and Methods

2.1. Overlaying of H13 Tool Steel on S355 Structural Steel

The base metal was a plate of commonly used S355 structural steel. On the surface of the plate, different configurations of layers of the H13 tool steel were welded using laser beam. For the purpose of welding, the H13 steel was in a powder state. Laser overlaying was performed at MATEX PM s.r.o. company.

As the first step, one layer of a single H13 surface track was welded on the plate surface – Figure 1. The second configuration was represented by the weld of five partially overlapping tracks. wherethe tracks were in a single layer. The third configuration was represented by five tracks like in the previous case, but in three layers, layer upon layer – Figure 1 at the bottom.

As regards the order of the tracks in case of five tracks overlays in Figure 1, the order is from top to bottom. That is why the bottom track is the widest, because it was welded as the last one, not partially overlapped by another track like the previous four ones.

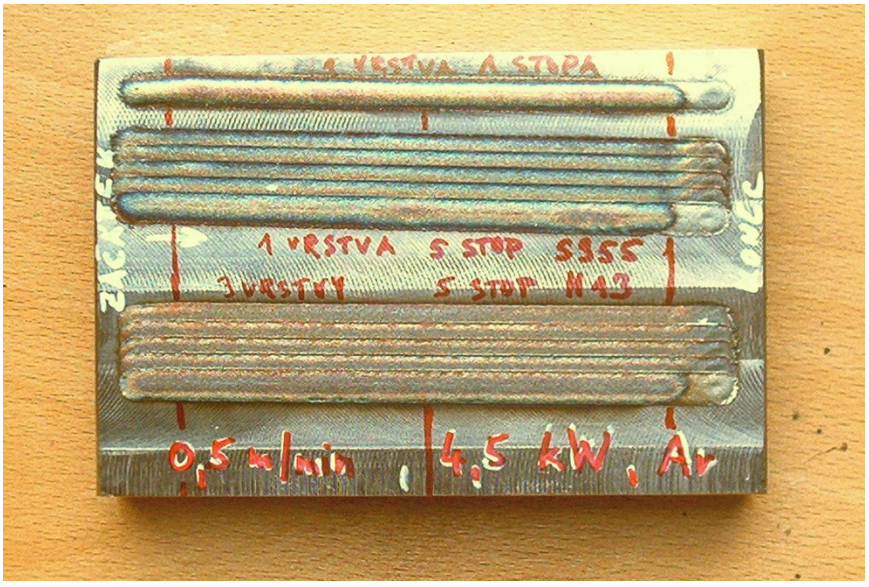

Figure 1. Total view of the first sample.

In all three cases, laser overlaying was carried out in a protective atmosphere of argon by laser beam of the power 4.5 kW. The beam surface speed was 0.5 m*min.

In the first step of experimental works, metallographic analyses were performed on transverse cuts of the plate with the welds. Metallographic samples were prepared by grinding and polishing. Macro- and microstructure was displayed by Villela-Bain metallographic etchant. Metallographic analyses were performed on the standard optical microscope Olympus.

Hardness of welded layers and courses of hardness were measured as HV10 Vickers hardness. Two directions of HV10 courses were evaluated, namely parallel or perpendicular to the surface, respectively. The parallel course was evaluated at the depth of several tenths millimeters from the surface, in both single layer and three layers welds. The perpendicular course comprised both values from the welds and base material.

 doi:10.20944/preprints202603.2365.v1

2.2. Overlaying of H13 Tool Steel on H11 Tool Steel

Overlaying of H13 Tool Steel on H11 Tool Steel was another research field. The importance of this knowledge arose from practice, when tools made of the H11 steel have to be repaired by further welding of the H13 steel. This welding technology was carried out at RAPTECH, s.r.o. company, which, however, has recently gone bankrupt. Nevertheless, the experimental project works have beensuccessfully finished, the bankruptcy affected neither the research project nor the results.

The overlaying of the AISI H13 powder on the base plate of AISI H11 (1.2343) tool steel was performed by diode laser Laserline of the maximum power 3 kW and Precitec laser head YW52 with four nozzles for powder feeding. The powder feeding was performed with the Model 1264 Powder Feeder with a possibility of preheating. The powder was preheated to 88 °C.

As before, different configurations of tracks were welded on two base plates of the H11 steel, namely tracks 1-4 on the first plate and tracks 5-7 on the second plate. Tracks 3 and 6 were welded with the same parameters, representing three multiple layers, layer upon layer, of five neighbouring tracks partially overlaying each other. The track 2 represented a single layer of five neighbouring tracks partially overlaying each other. In all cases, the mutual distance of axes was 1.7 mm, whilst the laser beam diameter was 2.8 mm.

Specimens of tracks 3 and 6 were examined from the point of view of macrostructure on metallographic optical microscope. Two specimens of track 3 and one specimen of track 2 were tested by fatigue.

2.3. Evaluation of Residual Stresses

Another field of research was targeted at evaluation of residual stresses caused by the welded layer. Residual stresses affect fatigue life and endurance limit particularly when different types of defects are present, like e.g. surface microscopic notches, pores, microcracks [4,16]. That is why residual stresses also were evaluated in this work. The measurement was carried out using a destructive method, with strain gauges. Residual stresses perpendicular to the weld tracks were evaluated. Two strain gauge (SG) chains Hottinger Baldwin MesstechnikHBM 1-KY11-4/120, the largest HBM chains, were used. The mutual distance of the SGs in the chain was 4 mm – Figure 2.

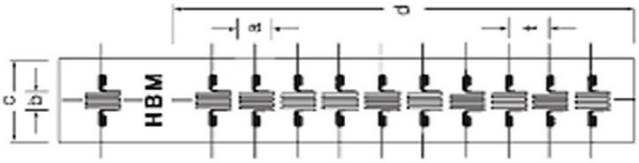

Figure 2. Scheme of HBM 1-KY11-4/120 strain gauges chains.

Placement of the strain gauge chains is shown in Figure 3. The first chain with SGs 1 – 10 was glued across the five double-layer overlay, in the bottom part of Figure 3. The first two strain gauges were outside the overlay, the third SG on the boundary between the widest weld track and base metal plate, the ninths SG on the opposite boundary and the tenth SG in the gap between the two five tracks overlays. As regards the second chain glued across the single-layer overlay, which was slightly narrower, the second SG was on the boundary, the seventh one on the gap between the overlay and the single weld on the top of Figure 3, SGs 8 and 9 on the boundaries of the weld. The SG 10 was near the margin of the single trace, on the base metal plate. Measured strains were evaluated using strain gauge device Hottinger Baldwin Messtechnik UPM60, which has an excellent temperature compensation and stability. The device was computer controlled and recorded.

 doi:10.20944/preprints202603.2365.v1

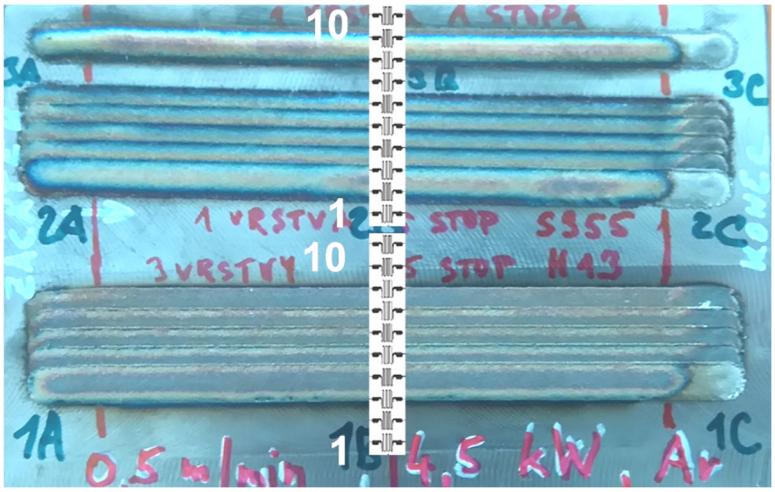

Figure 3. Position of strain gauge chains on the specimen.

The measurement was performed by sequential cutting of the welded sample and final removal of the base metal (BM) by turning. The principle consisted in the fact that before starting the cutting and material removal, the system of the base steel plate with the welds was balanced. The sequential cutting gradually changed this balance and after the final removal of all base metal by machining, the residual stresses relaxed and measured strains corresponded to absolute value of the stresses, with the opposite sign. Stresses were calculated from the strains using the E-modulus E = 206 GPa.

The cutting and material removal was carried out with the following steps:

- initial strain measurement after setting the strain gauge device to zero,
- cutting the bottom layer of BM to the thickness 4 mm,
- further cutting the bottom layer of BM to the thickness 2 mm,
- cutting of the specimen to three separate pieces – the part with double weld, the part with the single-layer weld and the part with the single weld track,
- machining all remaining BM off bellow all the welds.

After the final machining, all residual stresses were fully relaxed and original residual stresses could be simply calculated from the measured strains.

2.4. Fatigue Tests

Evaluation of fatigue properties was performed because of the need for knowledge about resistance of welded layers to fatigue loading, as cyclic loading is and important part of the service loading in such situations, besides thermal and wear loading.

Fatigue tests were performed on small specimens of approximately square cross section 7 x 7 mm or 9 x 9 mm under three-point bending – Figure 4. Test span was 35 mm. The central point of force was at the side opposite to the weld surface, which was therefore loaded by tensile stress with the maximum value at the centre decreasing to zero at the marginal points. In Figure 4, both double-layer specimen (left) and single layer (right) are shown. The supports and central point of load are indicated by red arrows. The specimens in Figure 4 are after fatigue cracking, which will be discussed in the section Results and Discussion.

 doi:10.20944/preprints202603.2365.v1

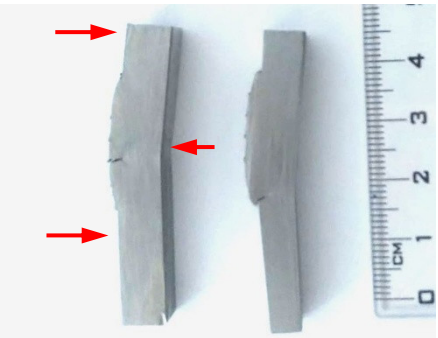

Figure 4. Three-point bending specimens used for fatigue tests.

Fatigue tests were performed on SCHENCK PHG high cycle fatigue machine with test frequency 40 Hz. In case of overlaying of the H13 steel on S355 base metal plate, the additively welded surface layers were in the as built state, with no machining or grinding. In case of overlaying of the H13 steel on the H11 tool steel, a thin surface layer of each specimen was ground off after careful measurement. The ground layer is indicated in Figure 5. The specimen axis was always perpendicular to the welding direction.

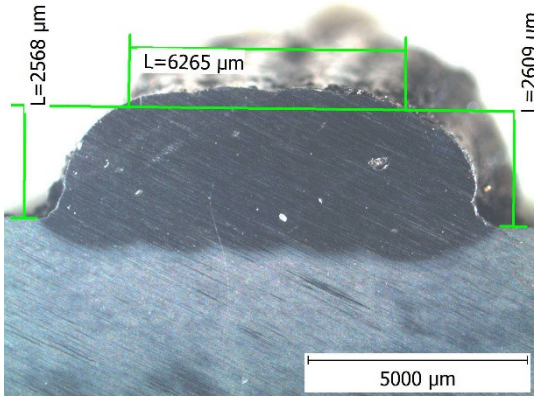

Figure 5. Example of grinding of the surface layer of the H13 welds on the H11 steel.

3. Results and Discussion

3.1. Optical Microscopy

Macrostructure and microstructure of the welds and base metal were analysed. In case of the H13 welds on the S355 steel plate, the quality of the welds was mostly acceptable, without pores or segregate impurities and with a good interconnection between the weld track and base material – Figure 6. Microstructure of the base material was, as supposed, ferritic-pearlitic, with uniform grain size – Figure 7. Heat affected zone was approximately 0.9 mm wide, refined in the direction to fusion zone, which was formed by martensitic structure. The welds were formed by martensitic structure of a dendritic type – Figure 8.

From the macroscopic point of view, problematic was the outer weld track, which contained pores and lacks of fusion – Figure 9.

 doi:10.20944/preprints202603.2365.v1

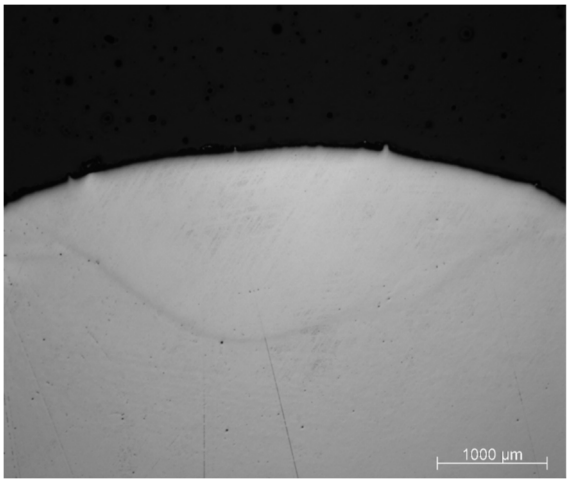

Figure 6. Single weld track on BM plate.

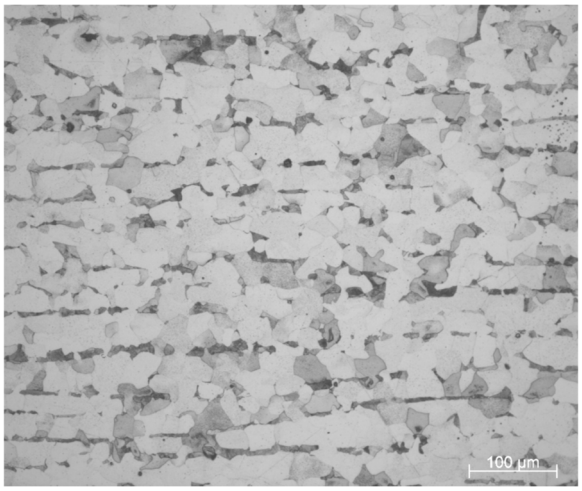

Figure 7. Ferritic-pearlitic microstructure of BM with uniform grain size.

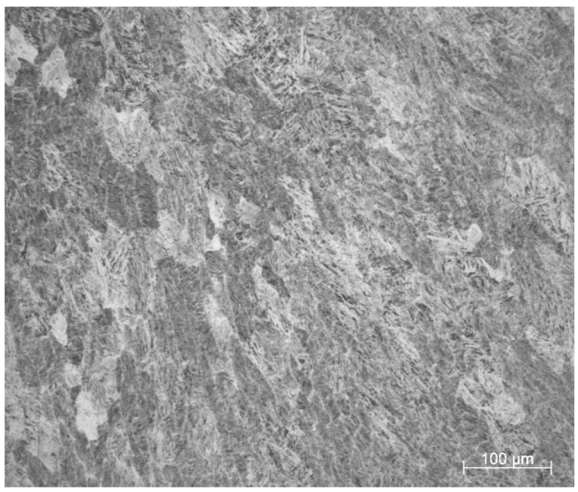

Figure 8. Weld martensitic microstructure of a dendritic type.

 doi:10.20944/preprints202603.2365.v1

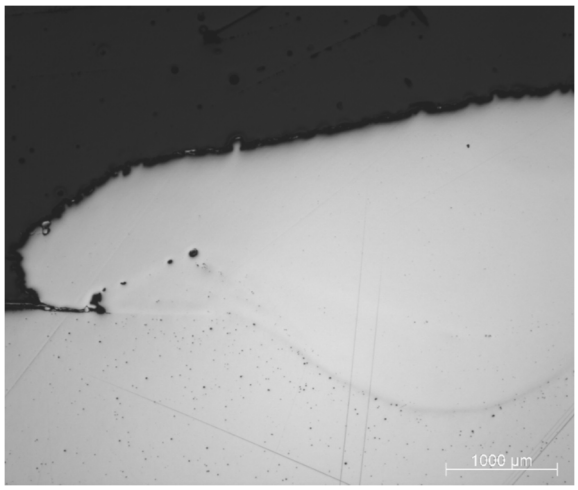

Figure 9. Outer weld track with pores and lacks of fusion.

Total views of macrostructure of the single weld and the single layer overlay with five tracks after etching are in Figures 10 and 11, respectively. Note lacks of fusion at track edges. which affected fatigue resistance and fatigue crack initiation, will be discussed later.

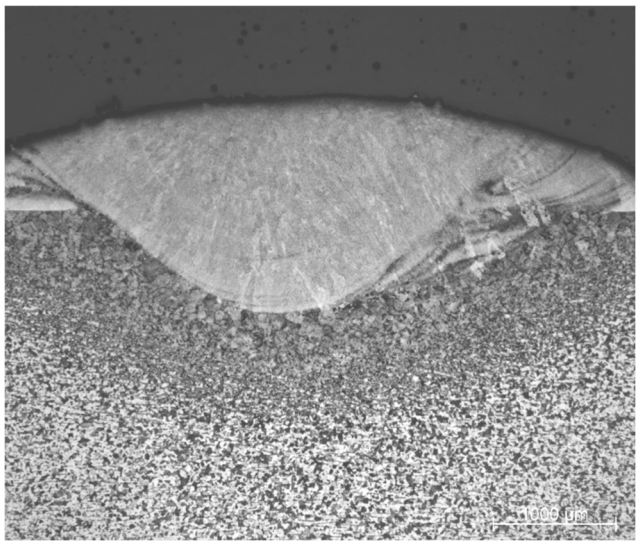

Figure 10. Macrostructure of single weld track after etching.

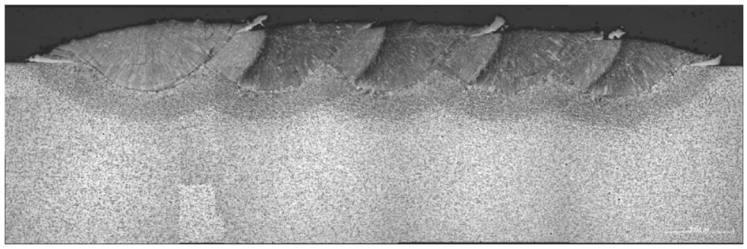

Figure 11. Macrostructure of single layer overlay with five tracks.

3.2. Evaluation of Hardness

The method of evaluation of HV10 hardness was described in section *2.1.*

The course of hardness perpendicular to the surface, i.e. in the direction from the surface through laser tracks to base material is shown in Figure 12.

 doi:10.20944/preprints202603.2365.v1

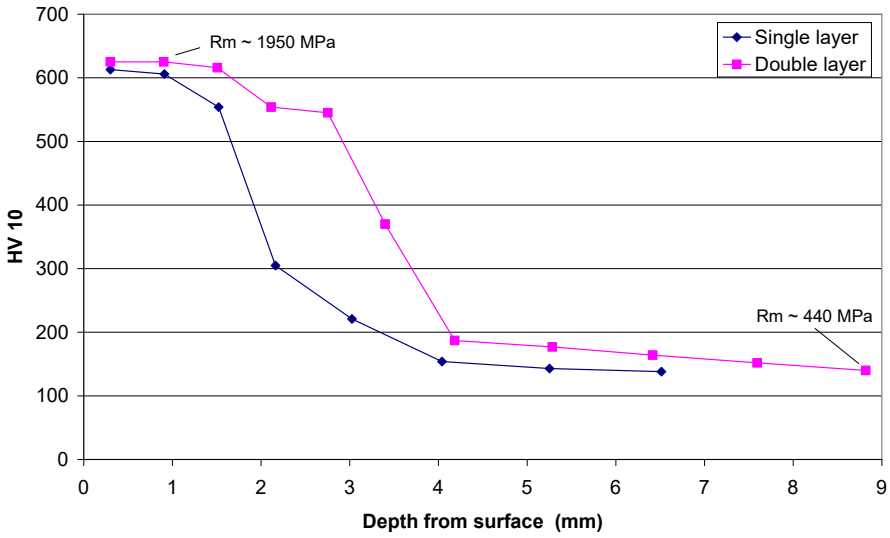

Figure 12. Course of HV10 hardness from the surface through welds to base material.

In Figure 12, maximum tensile strength values Rm estimated according to [20] for the maximum and minimum hardness, respectively, are shown, too. Note that the lowest strength 440 MPa, which corresponds to the base metal plate, is quite low, outside the range typical for the S355 steel 470 – 630 MPa [21] .

The courses of hardness in the direction parallel to the surface in both single layer track and double layer tracks are in Figure 13. It follows from the diagram that hardness values inside the overlaying tracks were always strongly affected by the next neighbouring track causing drop of hardness. Note that in Figure 12, tracks were welded from the right to the left, so the most left points in the diagram correspond to the last track, no more affected by further welding. The experimental points approximately correspond to the macrostructure photograph inserted into the diagram.

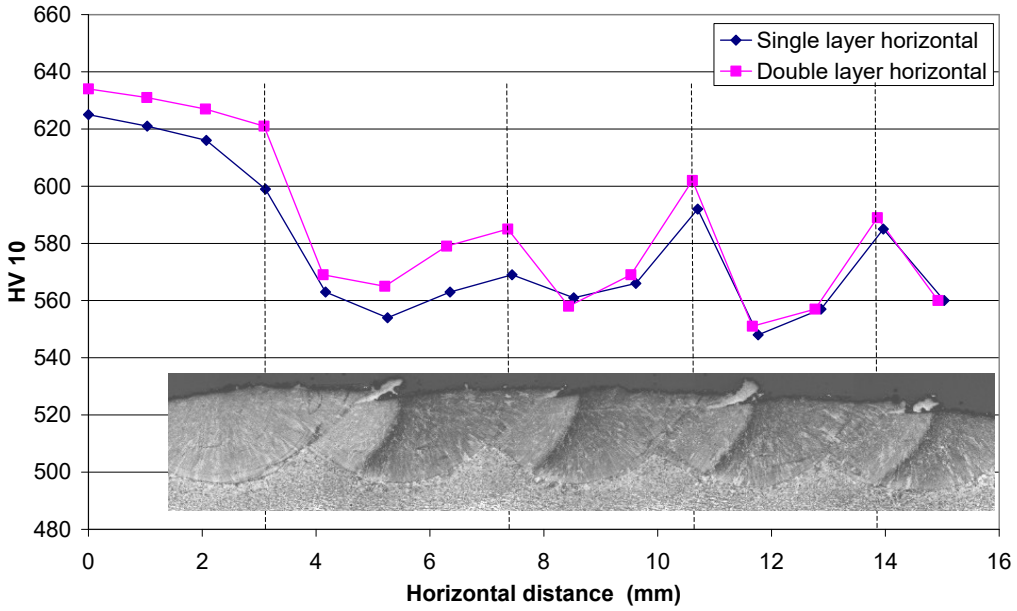

Figure 13. Courses of hardness in the direction parallel to the surface.

3.3. Analysis of Residual Stresses

The method of measurement of residual stresses is described in section 2.3. Effect of gradual machining on measured strains in double overlay is shown in Figure 14.

 doi:10.20944/preprints202603.2365.v1

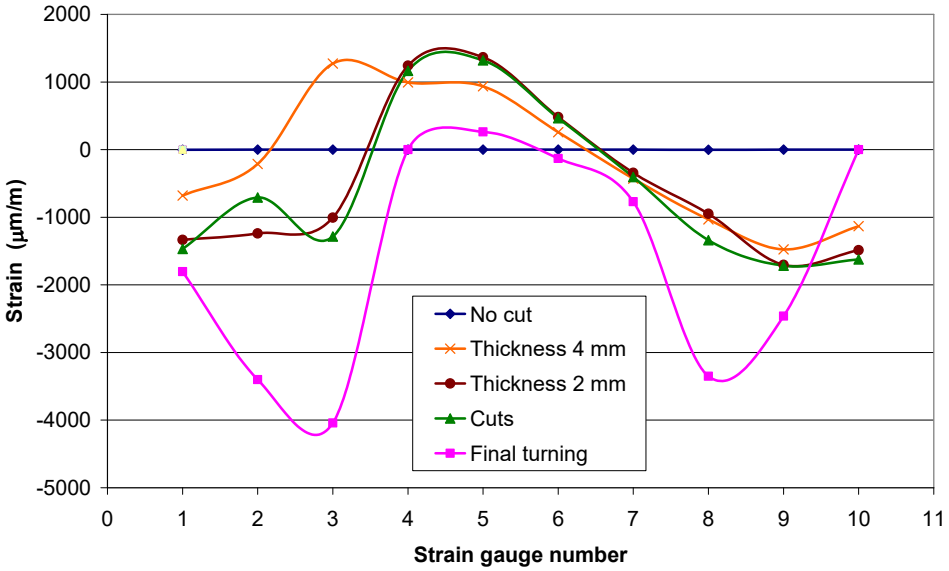

Figure 14. Strains measured at different stages of machining the material off.

The shape of the residual stresses curves in Figure 15 are logically consistent with the curves in Figure 14, they just have an opposite sign. Also note that when the machining of the base material was just partial, to the remaining thickness 4 mm, the residual stresses on the weld surface were slightly negative, giving evidence of a complex, complicated integral stresses distribution and balance in the weld and bellow it. Residual stresses reached into the base plate considerably and were balanced there. After the final machining, final turning, where the base metal was completely removed off, as indicated by the red dashed line in the macrostructure photograph in Figure 15, original residual stresses in the weld layer completely relaxed, resulting in the biggest negative measured strains. The corresponding positive peaks of the recalculated residual stresses were quite high, around 800 MPa, and were located at the marginal boundaries of the weld.

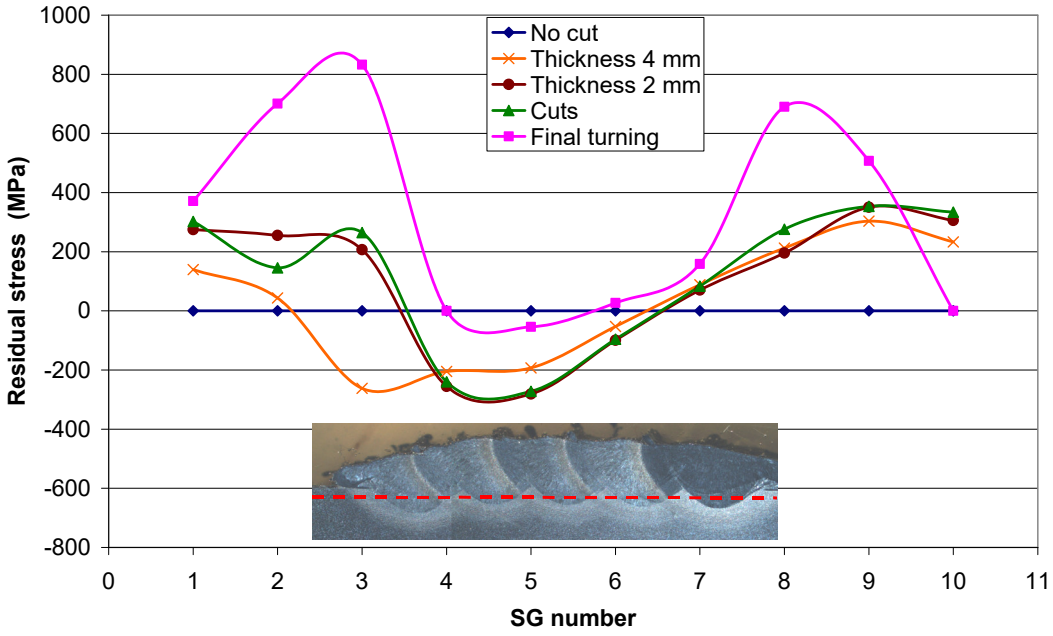

Figure 15. Original residual stresses recalculated from strains in Figure 13.

 doi:10.20944/preprints202603.2365.v1

Quite an important result is shown in Figure 16, namely residual stresses in the single layer overlay. The peak at the boundary of the first track was considerably higher than in case of the double layer weld, namely 1465 MPa. The peak on the opposite boundary was by contraries lower, only 370 MPa. The more uniform distribution of residual stresses in the double layer weld can be explained by the fact that during overlaying of the second weld, the original first layer was tempered resulting in reduction of the stresses. The comparison of residual stresses in the single and double layer overlays is in Figure 17. Note that the biggest value of residual stresses is quite close to the maximum strength of the weld evaluated from hardness, which was 1950 MPa. Such big residual stresses can considerably affect mechanical and particularly fatigue properties.

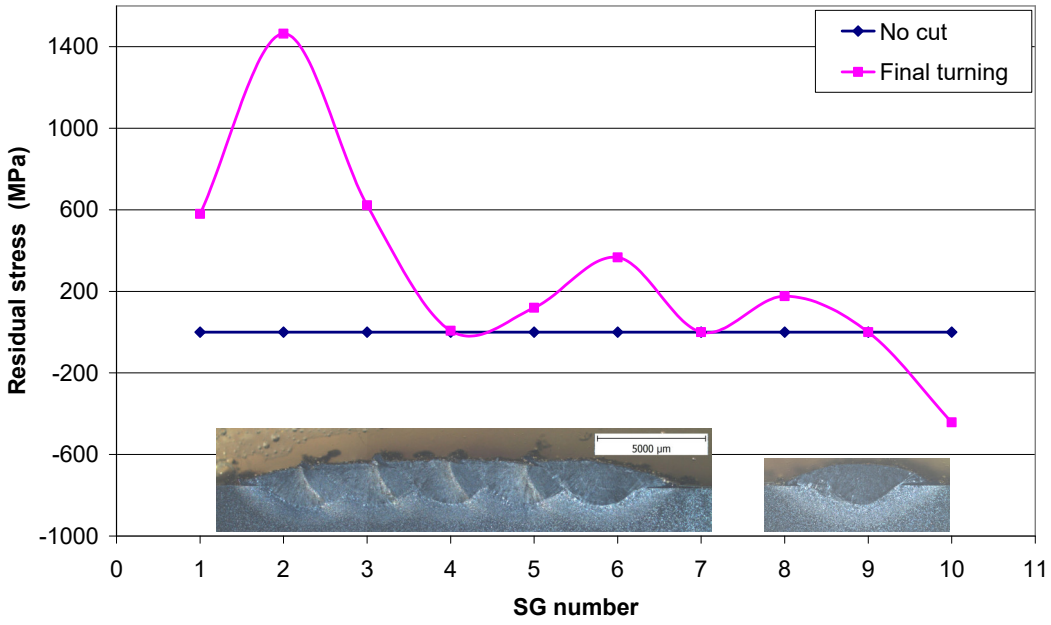

Figure 16. Original residual stresses in the single layer overlay and separate track.

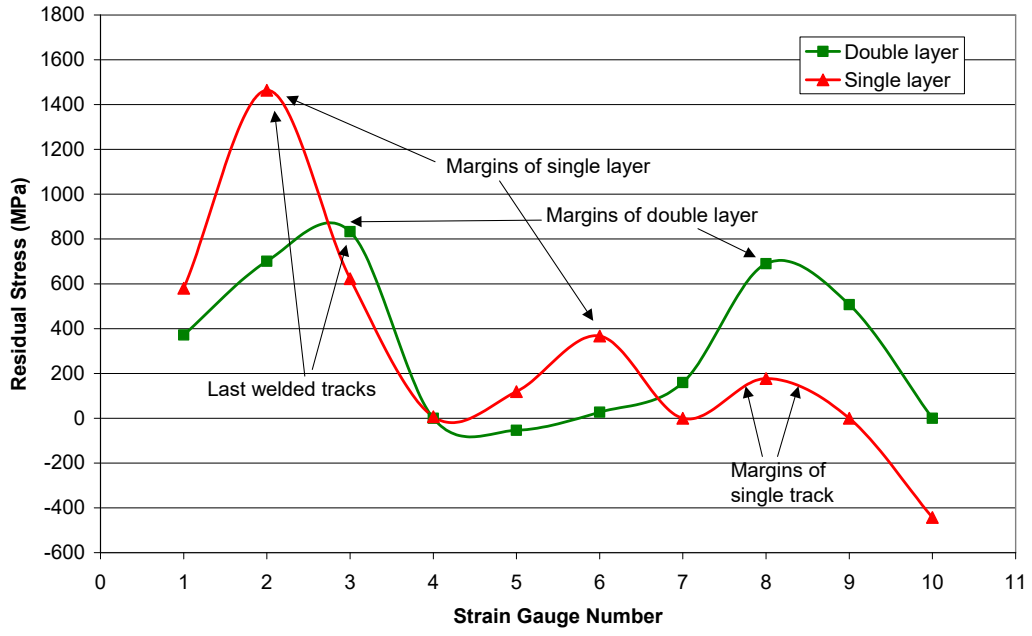

Figure 17. Comparison of residual stresses in single and double layer overlays.

 doi:10.20944/preprints202603.2365.v1

3.4. High-Cycle Fatigue Resistance and Fatigue Cracking Mechanisms

Results of high-cycle fatigue tests are shown in Figure 18.Stress range was calculated considering not only the nominal dimensions, but calculations were corrected and recalculated considering the actual specimen height at the cracking point including the overlay.

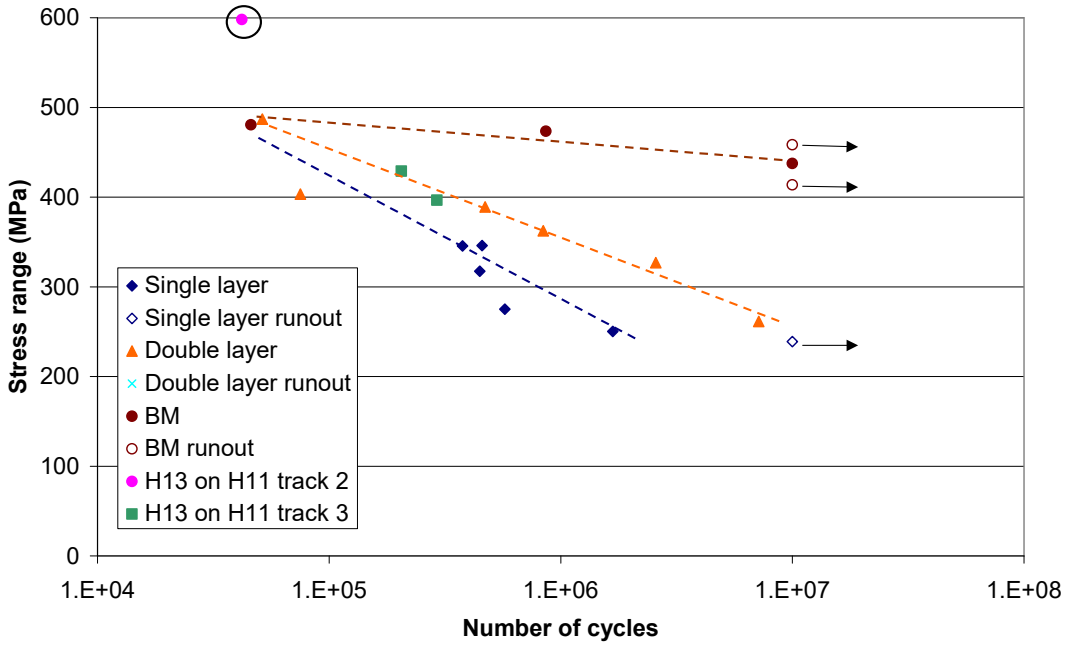

Figure 18. Results of high-cycle fatigue tests.

Fatigue strength of base material S355 steel was high. Fatigue strength of overlaid specimens was considerably lower, particularly in case of single layeroverlay. An interesting phenomenon is that fatigue life at fairly high stress range around 485 MPa is practically the same for almost all tested batches – base metal, double layer, single layer and also H13 weld on H11 tool steel. This indicates that fatigue life was affected by the properties of overlays, by resistance to fatigue crack initiation and early growth, rather than by the base metal. Number of cycles to failure at 485 MPa stress range was around 50000. Considering the thickness of overlay approximately 2 mm, then corresponding mean fatigue crack growth rate would be $4x10^{-8}$ m/cycle, which is a reasonable value, typical for region of stable crack growth [22]. Nevertheless, it would be interesting to evaluate fatigue crack growth (FCG) resistance of overlays mutually compared and compared to FCG of base metal. Unfortunately, such measurements were not possible within the performed research project carried.

In Figure 18, there are two points of premature failure, one concerns the double layer, one the single layer. The premature cracking probably occurred due to surface defects. Some of them, namely not completely welded powder particles, are documented in Figure 19. Another phenomenon worthy to discuss is the point with exceptionally high fatigue strength of the H13 double layer overlay on the H11 steel, namely stress range 598 MPa and 42000 cycles to failure. The point is indicated by circle. The likely explanation is a less occurrence of pores. In the single layer overlay on H11, there were probably less pores than in the multiple layers overlay, where pores were frequent – Figure 21. The fatigue strength is much higher than extrapolated S-N curve of single layer overlay. In single layer overlay,penetrating the weld layer by fatigue crack results in an immediate specimen failure due to the yielding of the rest of the specimen – the S355 material. Note that the weld thickness of the single layer is around 2 mm in comparison with 3.5 mm thickness of the double layer overlay – Figure 12. So, there is a considerably stronger support in the double layer overlay enabling a longer FCG phase. This hypothesis is supported by the rather surprising fact that experimental points of fatigue life of H13 steel do not depend on the base metal, either the S355 steel or the H11 tool steel. The points lie

 doi:10.20944/preprints202603.2365.v1

on the identical fatigue S-N curve. In addition, the fatigue life did not depend on the overlay surface state. As already mentioned, unlike overlays of the H13 steel on the S355 steel plate with no surface grinding, thin surface layers were ground off in case of overlaying the H13 steel on the H11 steel. Fatigue lives were identical no matter, whether fatigue cracks initiated on the surface defects in the former case or subsurface defects in the later case. It can be therefore concluded that fatigue life was determined by the resistance to short fatigue crack growth or notch sensitivity.

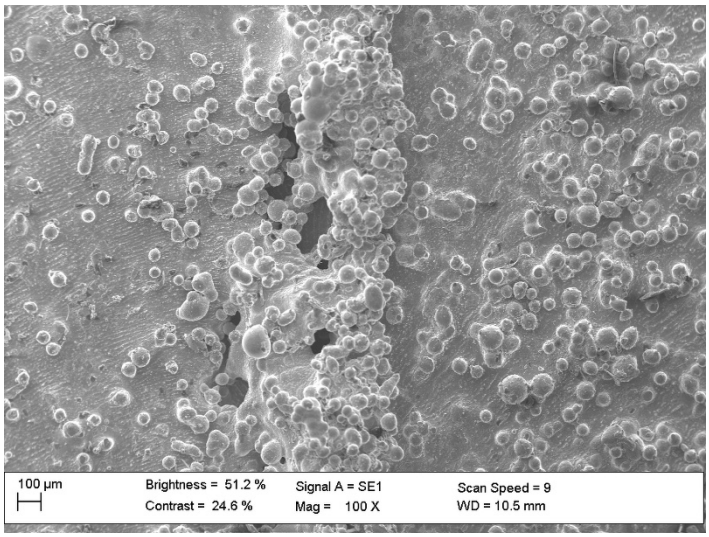

Figure 19. Example of surface defects on the single layer overlay.

Considering the residual stresses, their role is important particularly in case of FCG from surface notches and defects, where they reduce effects of crack closure. In case of smooth surface and defect-free material, their role is fairly minor as they affect mean stress, not stress range. An example is the right specimen in Figures 4 and 20, where cracking occurred at the notch at the overlay boundary with the residual stress peak 1465 MPa – Figure 17.

The last, but not least comment concerns defects, namely pores inside three layers overlay of the H13 on H11 tool steel, when the process parameters were not yet optimised – Figure 21. In this case, resistance of fatigue short cracks to growth was more critical factor than fatigue resistance of smooth defect-free specimens. This also explains, why fatigue life of H13 welds on H11 steel plate was equivalent to double layer H13 weld on the S355 plate, where fatigue cracks were initiated on the weld surface defects like in Figure 19.

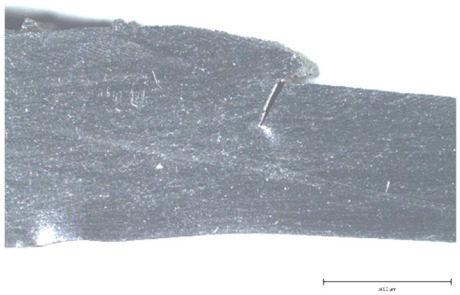

Figure 20. Fatigue crack initiated at the notch at the overlay boundary.

 doi:10.20944/preprints202603.2365.v1

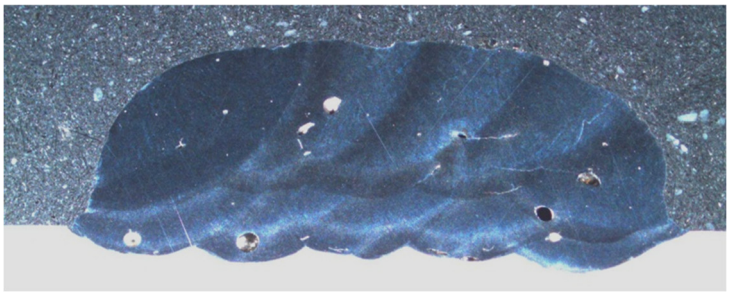

Figure 21. Pores inside five layers overlay of H13 on H11.

The most frequent failure mechanism is shown in Figure 22. Fatigue crack initiation on surface defects, namely not complete fusion of powder particles, followed by growth through the overlay. In Figure 22, the overlay is of the single layer type, of the thickness slightly bellow 2 mm. The fatigue life was determined by FCG through the overlays. That is why specimens with the double layer overlayof the thickness cca. 3.5 mm had higher fatigue life than the single layer specimens.

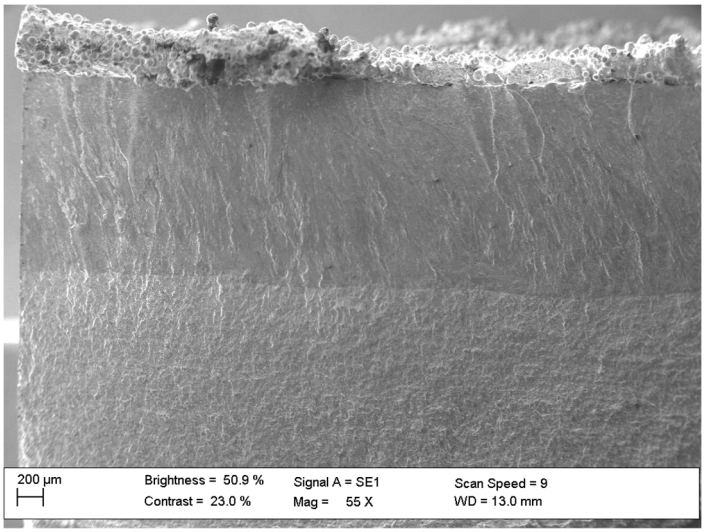

Figure 22. Fatigue crack initiation on surface defect and growth through single layer overlay of thickness 1.9 mm.

4. Conclusions

The aim of this work was an evaluation of properties of laser welded overlay of powder H13 steel on structural S355 steel, which is a cost effective solution, as the S355 steel is quite a non-expensive material. The second part of the project concerned welded overlay of powder H13 on H11 tool steel with the potential to be used for repairing of H11 tools like e.g. dies. The main conclusions can be summarized as follows:

In case of the H13 welds on the S355 steel plate, the quality of the welds was mostly acceptable, without pores or segregate impurities and with a good interconnection between the weld track and base material. Microstructure of the base material was ferritic-pearlitic, with uniform grain size. Heat affected zone was approximately 0.9 mm wide, refined in the direction to fusion zone, which was formed by martensitic structure. The welds were formed by martensitic structure of a dendritic type. Problematic was the outer weld track, which contained pores and lacks of fusion.

Tensile strength values Rmof overlays estimated from hardness corresponded to 1950 MPa in comparison with 440 MPa strength of the S355 base metal. The overlay thickness was 2 mm and 3.5 mm in case of the single layer and double layer overlays, respectively.

 doi:10.20944/preprints202603.2365.v1

High tensile residual stresses were measured at the boundary of the first track of the single layer overlay, namely 1465 MPa. The peak on the opposite boundary was considerably lower, only 370 MPa. Residual stresses in the double layer overlay were more uniform, between 700 and 860 MPa.

Fatigue strength of specimens with the single layer overlay was considerably lower than fatigue strength of the S355 steel. The decrease was between 25% to 50%. Fatigue strength of the double layer overlay on S355 steel was similar to that of the overlay on H11 steel. The decrease compared with the S355 steel was only between 25% and 30%. At high stress range, namely 480 MPa, there were almost no differences between all tested modifications.

Fatigue resistance of all overlaid specimens was affected by notch sensitivity and resistance of short cracks to growth from defects.

Author Contributions: Laser overlaying and specimen manufacture, Tomáš Mužík and František Wágner; microstructure analysis, hardness testing, High-cycle fatigue tests and SEM analysis, Jan Kec; residual stress evaluation, Ivo Černý; evaluation of fatigue resistance and damage mechanisms, Ivo Černý.

Funding: This research was funded by Technology Agency of the Czech Republic, grant number TG03010032-30-2.

Conflicts of Interest: The authors declare no conflicts of interest. The funders had no role in the design of the study; in the collection, analyses, or interpretation of data; in the writing of the manuscript; or in the decision to publish the results.

Abbreviations

The following abbreviations are used in this manuscript:

FCG	Fatigue Crack Growth
RS	Residual Stresses
AM	Additive Manufacturing
LB-PBF	Laser Beam – Powder Bed Fusion

References

1. Srinivas, M.; Babu, B.S. A Critical Review on Recent Research Methodologies in Additive Manufacturing. *Mater. Today Proc.* **2017**, Volume 4, Number 8, pp. 9049-9059. https://doi.org/10.1016/j.matpr.2017.07.258.
2. Herzog, D.;Seyda, V.; Wycisk, E.; Emmelmann, C. Additive manufacturing of metals. *ActaMaterialia***2016**, Volume 117, pp. 371-392. https://doi.org/10.1016/j.actamat.2016.07.019.
3. Elambasseril, J.; Rogers, J. ;Wallbrink, C. ; Munk, D. ; Leary, M.; Qian, M. Laser powder bed fusion additive manufacturing (LPBF-AM): the influence of design features and LPBF variables on surface topography and effect on fatigue properties. *Critical Reviews in Solid State and Material Sciences***2023**, Volume 48, Number 1, pp. 132-168. https://doi.org/10.1080/10408436.2022.2041396
4. Denti, L; Sola, A. On the Effectiveness of Different Surface Finishing Techniques on A357.0 Parts Produced by Laser-Based Powder Bed Fusion: Surface Roughness and Fatigue Strength. *Metals***2019**, Volume 9, Number 12. https://doi.org/10.3390/met9121284.
5. Segurajauregi, U.; Álvarez-Vázquez, A.; Muñiz-Calvente, M.; Urresti, I.; Naveiras, H. Fatigue Assessment of Selective Laser Melted Ti-6Al-4V: Influence of Speed Manufacturing and Porosity. *Metals***2021**, Volume 11, Number 7. https://doi.org/10.3390/met11071022.
6. Gu, D.; Shen, Y. Balling phenomena in direct laser sintering of stainless steel powder: Metallurgical mechanisms and control methods. *Mater, Des,***2009**, Volume 30, Issue 8, pp. 2903-2910. https://doi.org/10.1016/j.matdes.2009.01.013.
7. King, W.E.; Barth, H.D.; Castillo, V.M.; Gallegos, G.F.; Gibbs, J.W.; Hahn, D.E.; Kamath, C.; Rubenchik, A.M. Observation of keyhole-mode laser melting in laser powder-bed fusion additive manufacturing. *J. Mater. Process. Technol.***2014**, Volume 214, Issue 12, pp. 2915-2925. https://doi.org/10.1016/j.jmatprotec.2014.06.005.

8. Liu, Y.; Yang, Y.; Mai, S.; Wang, D.; Song, C.Investigation into spatter behavior during selective laser melting of AISI 316L stainless steel powder.*Mater. Des.* **2015,** Volume 87, pp. 797-806. https://doi.org/10.1016/j.matdes.2015.08.086.
9. Siddique, S.; Imran, M.; Rauer, M.; Kaloudis, M.; Wycisk, E.; Emmelmann, C.; Walther. F. Computed tomography for characterization of fatigue performance of selective laser melted parts.*Mater. Des.* **2015**, Volume 83, pp. 661-669. https://doi.org/10.1016/j.matdes.2015.06.063.
10. Akita, M.;Uematsu,Y.; Kakiuchi, T.; Nakajima, M.; Kawaguchi, R.; Defect-dominated fatigue behavior in type 630 stainless steel fabricated by selective laser melting.*Mater. Sci. Eng. A*,**2016**, Volume 666, pp. 19-26. https://doi.org/10.1016/j.msea.2016.04.042.
11. Wycisk, E.; Solbach, A.; Siddique, S.; Herzog, D.; Walther, F.; Emmelmann, C. Effects of defects in laser additive manufactured Ti-6Al-4V on fatigue properties.*Phys. Procedia*,**2014,** Volume 56,pp. 371-378. https://doi.org/10.1016/j.phpro.2014.08.120.
12. Yadollahi, A.;Shamsaei, N.; Thompson, S.M.; Elwany, A.; Bian, L. Effects of building orientation and heat treatment on fatigue behavior of selective laser melted 17-4 PH stainless steel.*Int. J. Fatigue***2017**, Volume 94, Part 2, pp. 218-235. https://doi.org/10.1016/j.ijfatigue.2016.03.014.
13. Brandl, E.;Heckenberger, U.; Holzinger, V.; Buchbinder, D. Additive manufactured AlSi10Mg samples using Selective Laser Melting (SLM): microstructure, high cycle fatigue, and fracture behavior.*Mater. Des.***2012**, Volume 34, pp. 159-169. https://doi.org/10.1016/j.matdes.2011.07.067.
14. Parareda, S.; Frómeta, D.; Casellas, D.; Sieurin, H.; Mateo, A. Understanding the Fatigue Notch Sensitivity of High-Strength Steels through Fracture Toughness. *Metals***2023**, 13(6), 1117; https://doi.org/10.3390/met13061117.
15. Cubi, R.E.; Gonçalves, R.L.P.; Massi, M.; Ribeiro, G.L.X.; Reis, L.; Couto, A.A. Comparison of Microstructure and Fatigue Life of Laser Powder Bed Fusion and Forging/Rolling Inconel 718 Alloy After Solution Heat Treatment and Double Aging. *Metals*
16. **2026**, 16(1), 57; https://doi.org/10.3390/met16010057.
17. Mancisidor, A.M.; García-Blanco, M.B.; Quintana, I.; Arrazola, P.J.; Espinosa, E.; Cuesta, M.; Albizuri, J.; Garciandia, F. Effect of Post-Processing Treatment on Fatigue Performance of Ti6Al4V Alloy Manufactured by Laser Powder Bed Fusion. *J. Manuf. Mater. Process.***2023**, 7(4), 119; https://doi.org/10.3390/jmmp7040119.
18. Blinn, B.; Klein, M.; Gläßner, C.; Smaga, M.; Aurich, J.C.; Beck, T. An Investigation of the Microstructure and Fatigue Behavior of Additively Manufactured AISI 316L Stainless Steel with Regard to the Influence of Heat Treatment. *Metals***2018**, 8(4), 220; https://doi.org/10.3390/met8040220
19. Černý, I.; Kec, J.; Poloch, A.; Zetek, M. Mechanical properties and high-cycle fatigue strength of 3D printed Inconel 718 alloy and effects of high-temperature exposure to corrosive atmosphere. *AIP Conf. Proc.* **2020,** Volume *2309*, Issue 1; https://doi.org/10.1063/5.0035400.
20. Elambasseril, J.; Rogers, J.; Wallbrink, C.; Munk D.; Leary, M.; Qian, M. Laser powder bed fusion additive manufacturing (LPBF-AM): the influence of design features and LPBF variables on surface topography and effect on fatigue properties. *Crit. Rev. Solid State Mater. Sci.***2023**, Volume 48, Issue 1, pp. 132-168. https://doi.org/10.1080/10408436.2022.2041396.
21. ČSN EN ISO 18265 Standard. Metallic materials – Conversion of hardness values. April **2014**. https://www.atreon.cz/jakost-s355/. Jakost S355 (ČSN 11523, St 52-3 U, Fe 510, ozn. W nr. 1.0547, 1.0553, 1.0554, 1.0570). Atreon, s.r.o., Čelákovice, Prague-East District, Czech Republic [in Czech].
22. ASTM E647-23a. Standard Test Method for Measurement of Fatigue Crack Growth Rates. April 05, **2024**. 43p.